Selected Papers from the Proceedings of the Fourth Geo-China International Conference

Geotechnical Special Publication No. 257

Advances in Numerical and Experimental Analysis of Transportation Geomaterials and Geosystems for Sustainable Infrastructure

Edited by
Rifat Bulut, Ph.D.
Xinbao Yu, Ph.D.
Shu-Rong Yang, Ph.D.

ASCE

G-I GEO-INSTITUTE

GEOTECHNICAL SPECIAL PUBLICATION NO. 257

GEO-CHINA 2016

ADVANCES IN NUMERICAL AND EXPERIMENTAL ANALYSIS OF TRANSPORTATION GEOMATERIALS AND GEOSYSTEMS FOR SUSTAINABLE INFRASTRUCTURE

SELECTED PAPERS FROM THE PROCEEDINGS OF THE FOURTH GEO-CHINA INTERNATIONAL CONFERENCE

July 25–27, 2016
Shandong, China

SPONSORED BY

Shandong University
Shandong Department of Transportation
University of Oklahoma
Chinese National Science Foundation
Geo-Institute of the American Society of Civil Engineers

EDITED BY
Rifat Bulut, Ph.D.
Xinbao Yu, Ph.D.
Shu-Rong Yang, Ph.D.

Published by the American Society of Civil Engineers

Reliability Analysis of Strain-Softening Slopes Using the First Order Reliability Method (FORM) 100
Subhadeep Metya, Gautam Bhattacharya, and Robin Chowdhury

Probabilistic Stability Analysis of Unsaturated Soil Slopes under Rainfall 108
Bai Tao and Deyu Zhang

Rainfall-Induced Failure of Volcanic Embankments Subjected to Cyclic Loadings in Cold Regions 116
Shima Kawamura, Seiichi Miura, Hieu Minh Dao, and Ryoichi Yamada

Computation of the Rotational Displacements of Gravity Retaining Walls by the Pseudo-Dynamic Method 124
Anindya Pain, Deepankar Choudhury, and S. K. Bhattacharyya

Statistical Correlations between Pressuremeter Tests and SPT for Glacial Tills 133
Kanagaratnam Balachandran, Jinyuan Liu, Laifa Cao, and Scott Peaker

Prediction of the Field Response of Soil-Support Systems in Deep Excavations 141
A. M. Hefny, T. M. Sorour, and M. E. Ezzat

Sustainable Mitigation of Slope Failure by Compacted Soil-Cement Fill 152
Jason Y. Wu, Kaiming Huang, and Munira Sungkar

A Numerical Approach to Solve 3D Geotechnical Problems with 2D Codes 160
Guangxian Hou and Shanzhi Shu

Risk Assessment Study on Long Oil and Gas Pipeline Construction-Induced Landslide Disasters 167
Mingzhou Bai, Yanqing Du, Zhihua Da, Yujian Xing, and Pingyuan Zhao

Probabilistic Assessment of Fill Slope Stability 175
Kelvin Lim, Alexander Schmid, and An-Jui Li

Probability of Liquefaction in Sabkha Soils under Different Earthquakes 183
Ahmed T. M. Farid

Site-Specific Seismic Response Analyses of a Municipal Solid Waste Dump Site at Delhi, India 191
B. J. Ramaiah, G. V. Ramana, and B. K. Bansal

Contents

Exploring the Geomechanics of Sinkholes: A Numerical Study of Sinkhole Subsidence and Collapse 1
Kishor Rawal, Zhong-Mei Wang, and Liang-Bo Hu

Reliability Assessment of Wedge Failure in Rock Slopes by the Random Sets Theory 9
Rodrigo Hernández-Carrillo and Gloria Inés Beltrán

Experimental and Numerical Analysis on the Specific Storage of Low Permeable Sandstone for Supercritical CO_2 18
Ardy Arsyad and Yasuhiro Mitani

Experimental Study on the Drained Shear Strength of Unsaturated Clayey Sand 35
Nigui Qian, Duanyi Wang, and Qingyan Tian

Application of the Low Strain Method to the Nondestructive Detection of the Integrity of Highway Bridge Rock-Socketed Piles 43
Laisheng Xue and Xiangxing Kong

Performance Evaluation of Pier Foundation Excavations at an Existing Freeway Embankment 50
James C. Ni and Wen-Chieh Cheng

Microstructural Damage-Induced Localized Fracturing of Brittle Rocks 58
Tao Xu, Shengqi Yang, Mike Heap, Chongfeng Chen, and Tianhong Yang

Numerical Simulation of Built-In Oblique Circular 3D Crack Propagation under Uniaxial Compression by the Element Free Galerkin Method 66
Dun-Fu Zhang, Sheng-Hua Huang, Bo Zhang, Shu-Cai Li, and Wei-Shen Zhu

Seismic Stability Analysis of Un-Reinforced and Reinforced Soil Slopes 74
S. Sahoo, B. Manna, and K. G. Sharma

Use of Retaining Walls with Relief Shelves as an Economic Solution 82
Hany Farouk Shehata

Effect of Supporting Soil Rigidity on the Apparent Earth Pressure 91
Hany Farouk Shehata and Tamer M. Sorour

Preface

This Geotechnical Special Publication (GSP) contains 23 papers addressing a variety of current issues in Soils and Rock Instrumentation, Behavior, and Modeling; Earth Retaining Walls and Slope Stability; and Seismically Induced Hazards and Mitigation. These papers were presented at the GeoChina International Conference held on July 25-27, 2016 in Shandong, China. The technical programs for the GeoChina International Conference struck a balance between the fundamental theories and field applications. Sustainable civil infrastructures using innovative technologies and materials are endorsed by a number of leading international professional organizations. This GSP includes investigations and solutions from numerous countries. It expands ranges of tools that are available to engineers and scientists.

Acknowledgments

The following individuals have assisted in reviewing the papers:

Tejo vikash Bheemasetti, Sao-Jeng Chao, Cheng-Wei Chen, Lizhou Chen, Xiang Chen, Yi Dong, Ceki Harman, G.T. Hong, Quan Gao, Jeffrey Lee, Zhen Liu, BooHyun Nam, Fatih Oncul, Aravind Pedarla, Asheesh Pradhan, Elmira Riahi, Hakan Sahin, Zhiming Si, Xiaoming Yang, Xinbao Yu, Bin Zhang, and Nan Zhang.

Published by American Society of Civil Engineers
1801 Alexander Bell Drive
Reston, Virginia, 20191-4382
www.asce.org/publications | ascelibrary.org

Errata: Errata, if any, can be found at http://dx.doi.org/10.1061/9780784480007

ISBN 978-0-7844-8000-7 (PDF)
Manufactured in the United States of America.

Experimental and Numerical Analysis on the Specific Storage of Low Permeable Sandstone for Supercritical CO_2

Ardy Arsyad[1] and Yasuhiro Mitani[2]

[1]Dept. of Civil Engineering, Faculty of Engineering, Hasanuddin Univ., Makassar 90245 Indonesia. E-mail: ardy.arsyad@unhas.ac.id

[2]Dept. of Civil and Structural Engineering, Graduate School of Engineering, Kyushu Univ., Fukuoka 0819-0395, Japan. E-mail: mitani@doc.kyuhu-u.ac.jp

Abstract: Experimental tests and numerical analysis were undertaken to investigate the specific storage of sedimentary rocks for supercritical CO_2. New laboratory system of constant flow pump permeability test was developed in order to measure permeability and specific storage of sedimentary rock in similar physical condition of deep aquifer where CO_2 tends to be in supercritical phase. To analyze experimental results, numerical analysis was established by extending the theoretical model of constant flow permeability to deal with two phase flow drainage displacement. For the examination of its applicability, experimental test was undertaken in which Ainoura sandstone used as core sample, injected with supercritical CO_2 under laboratory condition of 35°C constant reservoir temperature, 10 MPa initial hydraulic pressure, and 20 MPa constant overburden pressure The experimental results show that, average specific storage of Ainoura sandstone is about 3.74×10^{-4} 1/Pa at a maximum CO_2 saturation of 0.55, and volumetric strain increases about 0.7%. The accuracy of specific storage measured was validated with ratio of the specific storage of the sandstone to the storage capacity of the pump used in the permeability test. This finding suggested that newly developed constant flow pump technique with its numerical analysis can be used to effectively obtain specific storage of sedimentary rock for CO_2 in supercritical phase.

INTRODUCTION

CO_2 sequestration in deep saline aquifers has become one of the most viable options to reduce the emission of anthropogenic greenhouse gases into the atmosphere. In Japan, deep sedimentary basins have been considered as suitable media for CO_2 sequestration since sedimentary formations comprise over half of Japan's total subsurface geology, with an estimated 146 billion Gt-CO_2 storage capacity (Ogawa et al. 2011; Nakanishi et al. 2009; Takahashi et al. 2009). However, prior to the commercialization of CO_2

sequestration projects in sedimentary basins, detailed studies were needed to understand the physics of water-CO_2 flow in this type of geological environment. In fact, CO_2-brine multiphase flow data is rather scarce compared to oil-water and CO_2-oil multiphase flow data generated for oil reservoirs over decades (Perrin and Benson 2010). Relative permeability and specific storage can be determined by two phase differential pressures and individual phase flow rates using Darcy's law. The injection ratio of the two-phase fluid is repeatedly alternated in order to determine the relative permeabilities at different saturation levels. A number of studies have been undertaken in measuring CO_2-water relative permeability and storativity in sedimentary rocks (Bennion and Bachu (2005), Perrin et al., (2009), and Shi et al. (2009). However, accurate, repeatable, and reliable relative permeability measurement with standardized and comparable laboratory experiments remains a research subject (Müller, 2011).

A standard experimental method used for permeability measurement is constant flow pump permeability test. This method is introduced by Olsen et al. (1985) as an improved version of the transient flow method introduced by Brace et al. (1968). The principle work of the flow pump permeability is to generate a constant rate of flow to precisely control pore fluid transport processes in a specimen. The flow of fluid through the specimen generates a hydraulic head that transiently increases and subsequently stabilizes to steady state with a constant head gradient imposed across the specimen. By using Darcy's law, the corresponding permeability value can be determined based on the steady state data collected. However, it would take several hours to reach steady state for the condition of a large specimen or a large pump system. Morin and Olsen (1987) developed a mathematical model for transient pressure response by considering the storage capacity of the specimen. This enables the determination of the permeability in early testing time. Later, Esaki et al. (1996) introduced the effect of storage capacity of the pump system to enhance the accuracy and efficiency of the mathematical model. Song et al. (2004) then introduced a more efficient and less tedious method to Esaki's et al. (1996) numerical simulation. In general, the constant flow pump permeability method is employed to measure the hydraulic conductivity and specific storage of rocks at laboratory conditions. In this study, we endeavor to develop laboratory system of the constant flow pump permeability method and its numerical analysis in order to measure permeability and specific storage of rock under the injection of CO_2 in supercritical phase. The validity and applicability of this technique are also included in this paper.

Experimental System

Figure 1 shows the schematic diagram of flow pump permeability test in the new developed experimental system. The new experimental system consists of several developed apparatus such as temperatures controllers, pressure controllers, and flow controllers. The aim of this instalment is to generate and stabilize high temperature and high pressure desired to create reservoir condition where CO_2 is in supercritical state. The main difficulty in creating a reservoir condition with high pressure and high

temperature is the vulnerability of the experimental system to the unstable temperature associated with seasonal weather and heat induced by the experiment apparatus. Such condition will affect the physical property of CO_2 leading to inaccuracy of experimental measurement. Therefore, the external and internal lab temperatures were attempted to control by constructing a greenhouse chamber and installing several devices and apparatus such as those are listed as follows: thermostatic room, greenhouse chamber, hemathermal circulation tank, and constant temperature water tank, temperature controller for pressure vessels, thermocouple and heater bars, remote control, and data acquisition system. Strain gauges were employed to measure deformation of rock specimen (Figure 2). The strain gauges were attached laterally and longitudinally on rock specimen.

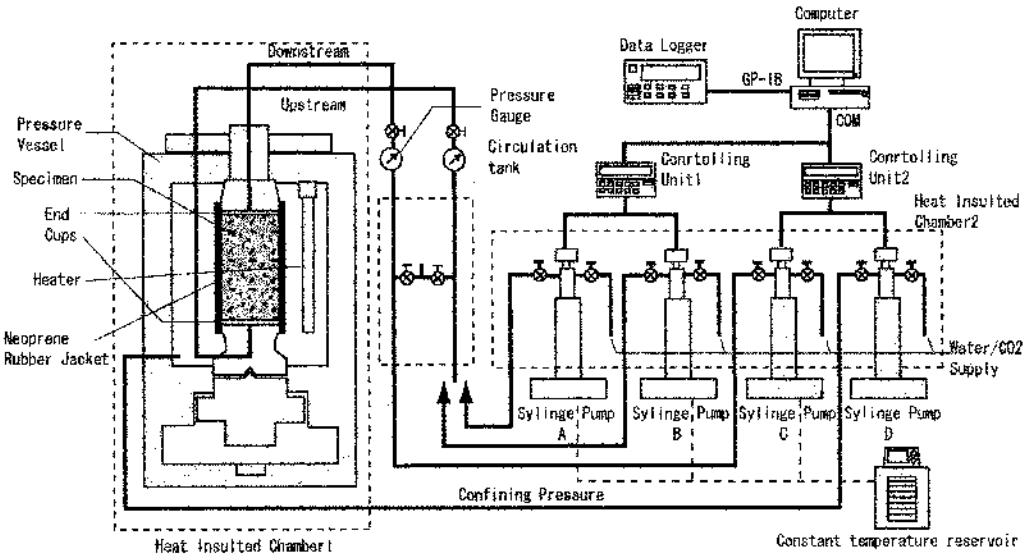

FIG. 1. Schematic diagram of constant flow pump permeability with newly developed laboratory system.

Rock specimens used in the experiments are Ainoura sandstones obtained from Sasebo, near Nagasaki Prefecture in Japan. The sandstone is a low permeable but high porosity rock, expected to be suitable for CO_2 storage. The pore size distribution of the Ainoura sandstone was investigated by using Pore Analyzer (Porosimeter) Micrometritics Auto pore III. Figure 3 presents the pore size distributions of the Ainoura sandstone specimens. It can be seen that two different Ainoura samples (Ainoura 1 and 2) exhibited a bi-modal pore size distribution, indicating heterogeneous pore siliciclastic characteristics. Due to the larger microporosity of Ainoura 1 than Ainoura 2 (Table 1), Ainoura 1 appeared to contain a much finer grain matrix than Ainoura 2. Figure 4 presents CO_2-water capillary pressure of Ainoura 1 and 2 specimens. By fitting the capillary pressure data with the Van Genuchten (1980) equation, the irreducible water saturation, S_{wr}, threshold capillary pressure, P_o, and pore size index, m.

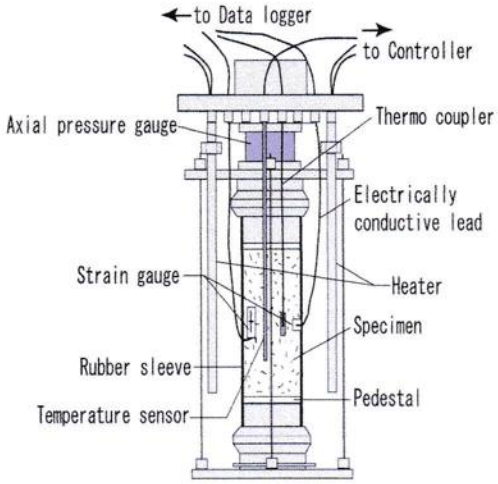

FIG. 2. Rock specimen with strain measurement devices and temperature controller.

Table 1. Pore Size Characteristics in the rock specimens

Specimen	% Micro-pores	% Mesopores	% Macropores	Median pore size (μm)	Porosity	IFT (mN/m)	P_0 (kPa)
Ainoura 1	64.7	22.1	13.1	1	12.6	32.1	27
Ainoura 2	51.06	29.4	19.6	1.2	15.46	32.1	25

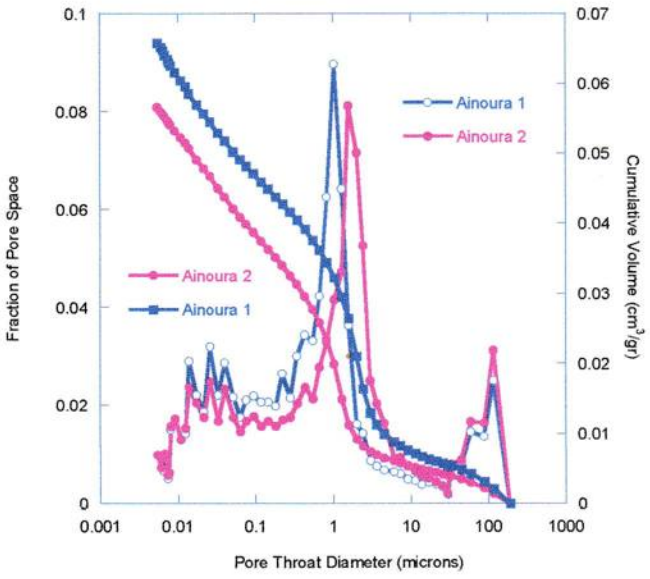

FIG. 3. Pore size distribution of Ainoura sandstone specimens.

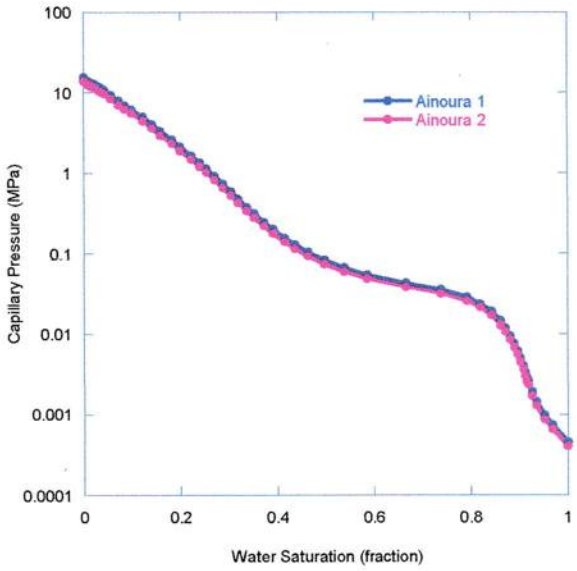

FIG. 4. Capillary pressure of Ainoura sandstone specimens.

Figure 5 illustrates the experimental system of the injection of supercritical CO_2 into the Ainoura sandstone by using the flow pump permeability test. To maintain the physical characteristic of CO_2 in the supercritical phase, the temperature of rock specimen, syringe pumps, syringe pipes and pressure vessels were maintained at 35°C, 36°C, and 38°C, respectively. After the temperatures stabilized, the confining pressure of 20 MPa and the pore pressure of 10 MPa were subjected on the specimen. The supercritical CO_2 within 3 μl/min flow rate was injected into the rock specimen and the pressures generated by the injection were measured continuously. The precision of the measurement can be seen from the record of the pressure in outlet and inlet of the rock specimen for every two seconds. Therefore, the pressure data of around 24 million during the experiment can be obtained. The measurement of the generated pressure was performed by employing the pressures of two gauges with resolution of 50 cmH2O or 0.0049 MPa, manufactured by Research Institute Tokyo.

During the injection, the generated hydraulic pressures in the upstream and downstream of the Ainoura sandstone specimen including its volumetric strain were measured (Figures 6 and 7). The flow of the injected CO_2 generated an increase in pore pressure while the differential pressure was dropping. Meanwhile, the increase in the pore pressure propagated a deformation on the Ainoura sandstone specimen. The negative direction of the increasing strains indicates such an expansion of the Ainoura sandstone specimen.

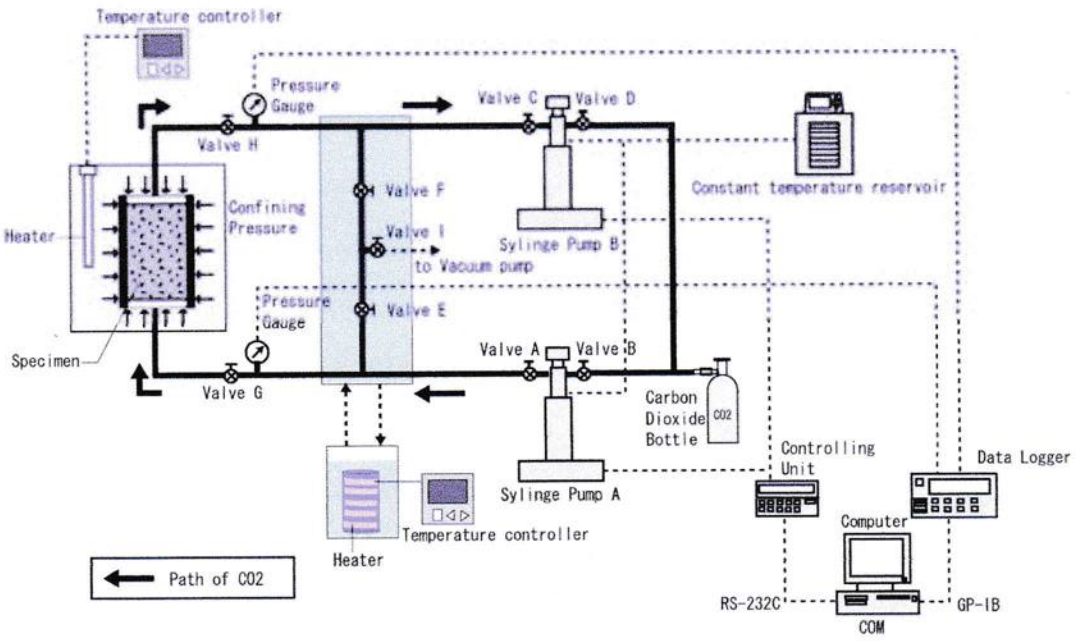

FIG. 5. Schematic diagram of experimental test of CO2 injection.

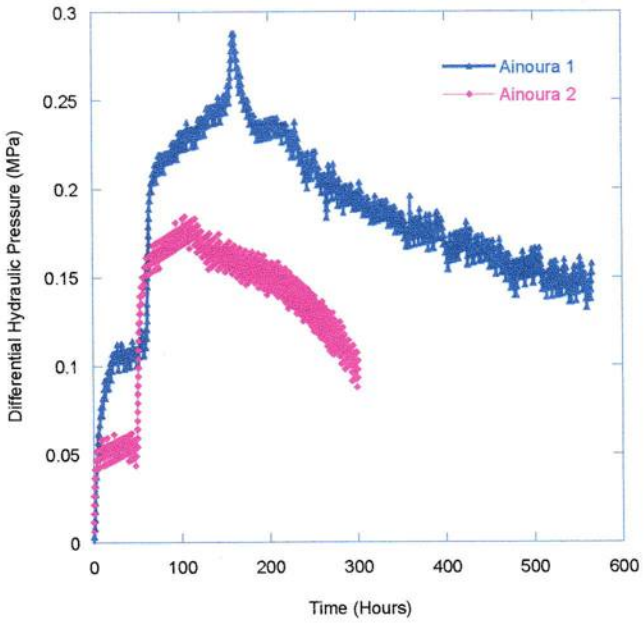

FIG. 6. Measured differential pressure between upstream and downstream side of the rock specimen during CO_2 injection.

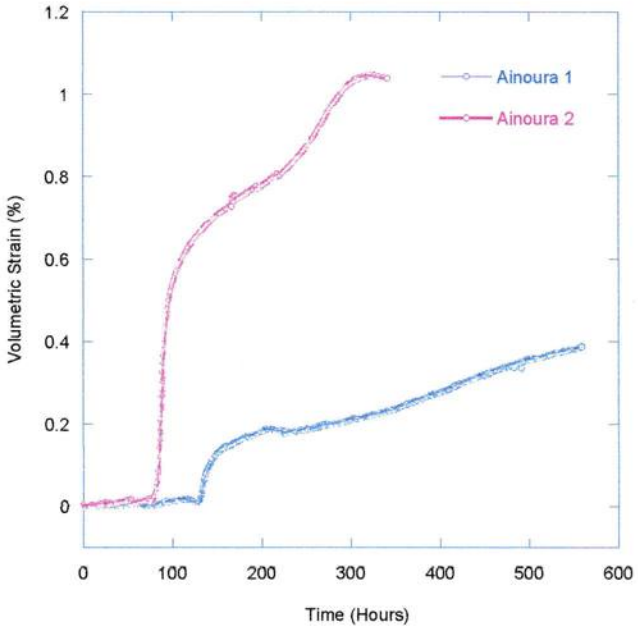

FIG. 7. Measured volumetric strain of the rock specimen propagated by CO_2 injection.

Theoretical model

The mathematical model of the flow pump permeability test is described as one-dimensional transient flow of a compressible fluid through a saturated porous and compressible medium. This model combines the principle of fluid mass in a deformable matrix and Darcy's law for laminar flow through a hydraulic isotropic rock matrix (Zhang et al. 2000). Since the experimental system of CO_2 injection into low permeable rock saturated with water can be described as a two-phase flow drainage displacement process, volumetric balance can be employed. It can be assumed that, after breakthrough, the flow rate of the injected fluid is equal to the total flow rate of the displaced and displacing fluid. Due to the compressibility of the displacing fluid (which is a liquid-like gas), the assumption was that the flow rate of the injected fluid was the total of the displaced fluid, and the displacing fluid, at time t minus volume, was absorbed within the compressible pump system per unit time interval. The system included the entire space of the flow pump cylinder, the space in the lower pedestal, and the tubing connecting the flow pump to the test cell. This assumption also led to the change of the boundary conditions of the model shown in Eq. 4 and 4a. The schematic diagram and boundary conditions associated with the modified mathematical model are depicted in Figure 8.

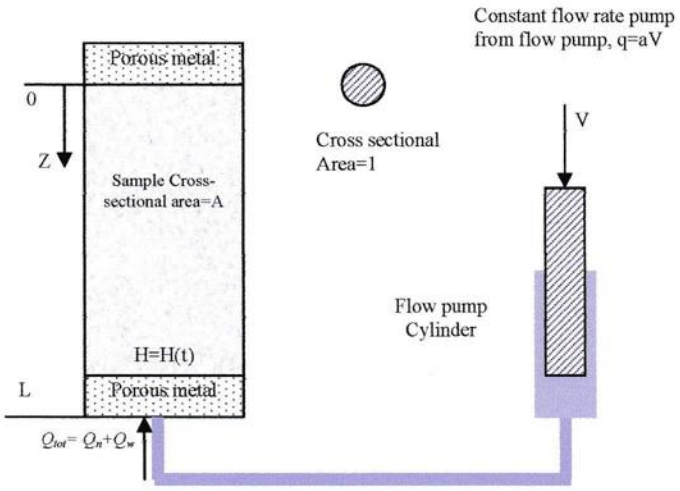

FIG. 8. Schematic diagram of the theoretical model of constant flow pump permeability test.

The governing equation is defined as follows:

$$\frac{\partial^2 H_n}{\partial z^2}-\frac{S_s}{k}\frac{\partial H_n}{\partial t}=0 \tag{1}$$

Initial condition:

$$H(z,0)=0 \qquad 0\le z\le L \tag{2}$$

Boundary conditions:

$$z=0,\ H(0,t)=0 \qquad t\ge 0 \tag{3}$$

$$z=L,\ Q(t)=Q_n(t)+Q_w(t) \tag{4}$$

$$Q(t)=\left(\frac{k_{rn}}{\mu_n}\frac{dH_n}{dz}\rho_n+\frac{k_{rw}}{\mu_w}\frac{dH_w}{dz}\rho_w\right)gKA \tag{4a}$$

where H = hydraulic pressure, *MPa*,
H_w = hydraulic pressure of water, *MPa*,
H_n = hydraulic pressure of CO_2, *MPa*,
k = hydraulic conductivity, cm/s,
z = vertical distance along the specimen, cm,

t – time from the start of the experiment, s,
S_s = specimen's specific storage, 1/Pa,
K = intrinsic permeability of the specimen, cm^2
k_{rw} = relative permeability of water, fraction,
k_{rn} = relative permeability of CO_2, fraction,
L = the length of the specimen, cm,
μ_w = dynamic viscosity of water, $Pa.s$,
μ_{nw} = dynamic viscosity of CO_2, $Pa.s$,
ρ_w = density of water, gr/cm^3,
ρ_n = density of CO_2, gr/cm^3,
A = the cross-sectional area of the specimen, cm^2,
$Q(t)$ = flow in the specimen at time t, cm^3/s,
$Q_n(t)$ = flow of CO_2 in the specimen at time t, cm^3/s,
$Q_w(t)$ = flow of water in the specimen at time t, cm^3/s,
g = gravity acceleration, cm/s^2

Since $\frac{dH_w}{dz} = \frac{dH_n}{dz} - \frac{dH_c}{dz}$, equation (4a) can be described as:

$$Q(t) = \left(\frac{k_{rn}}{\mu_n}\rho_n + \frac{k_{rw}}{\mu_w}\rho_w\right)\frac{dH_n}{dz}gKA - \frac{k_{rw}}{\mu_w}\rho_w\frac{dH_c}{dz}gKA \qquad t>0$$

Hence, the displacing non-wetting fluid pressure gradient becomes:

$$\frac{dH_n}{dz} = \frac{Q(t)}{\left(\frac{k_{rn}}{\mu_n}\rho_n + \frac{k_{rw}}{\mu_w}\rho_w\right)gKA} + \frac{\frac{k_{rw}}{\mu_w}\rho_w\frac{dH_c}{dz}}{\left(\frac{k_{rn}}{\mu_n}\rho_n + \frac{k_{rw}}{\mu_w}\rho_w\right)}$$

In which

$$\int_0^t Q(t)\,dt = \int_0^t q\;dt - C_e H_n(L,t)$$

$$\therefore\; Q(t) = q - C_e\frac{dH_n(L,t)}{dt}$$

Where

q = CO_2 flow rate into the upstream of the specimen at time t, cm^3/s,
C_e = storage capacity of the flow pump system, i.e., the change in volume of the permeating fluid in upstream permeating system per unit change in hydraulic head, cm^3/cmH_2O

The complete analytical solution is give as follows:

$$h(z,t)=\frac{qL+\left(gKA\dfrac{k_{rw}}{\mu_w}\rho_w L\dfrac{dH_e}{dz}\right)}{KAg\left(\dfrac{k_{rn}}{\mu_n}\rho_n+\dfrac{k_{rw}}{\mu_w}\rho_w\right)}\left\{\frac{z}{L}-2\sum_{n=1}^{\infty}\frac{\exp\left(-\dfrac{K\left(\dfrac{k_{rn}}{\mu_n}\rho_n+\dfrac{k_{rw}}{\mu_w}\rho_w\right)}{S_s}\beta_n^2 t\right)\sin(\beta_n z)}{L\delta\beta_n\cos(\beta_n L)\left[L\left(\beta_n^2+\dfrac{1}{\delta^2}\right)+\dfrac{1}{\delta}\right]}\right\} \quad (5)$$

Where $\delta=\dfrac{C_e}{AS_s}$, and β_n is the root of following equation:

$$\tan\phi=\frac{1}{\delta\beta^2}\left(k_{rw}+k_{rn}\frac{\mu_w\rho_n}{\mu_n\rho_w}\right)$$

The roots were obtained using the Newton Raphson Method (Carslaw and Jaeger 1959).

The hydraulic gradient distribution within the specimen can be further derived by differentiating Eq. (5) with respect to variable z:

$$i_n(z,t)=\frac{qL+\left(gKA\dfrac{k_{rw}}{\mu_w}\rho_w L\dfrac{dH_e}{dz}\right)}{KAg\left(\dfrac{k_{rn}}{\mu_n}\rho_n+\dfrac{k_{rw}}{\mu_w}\rho_w\right)}\left\{\frac{1}{L}-2\sum_{n=1}^{\infty}\frac{\exp\left[-\dfrac{K}{S_{sn}}\left(\dfrac{k_{rn}}{\mu_n}\rho_n+\dfrac{k_{rw}}{\mu_w}\rho_w\right)\beta_n^2 t\right]\cos(\beta_n z)}{L\delta\beta_n\cos(\beta_n L)\left[L\left(\beta_n^2+\dfrac{1}{\delta^2}\right)+\dfrac{1}{\delta}\right]}\right\} \quad (6)$$

CO_2-water relative permeability

History curve matching between the pressure gradient from the experiment and the corresponding data of pressure gradient based on theoretical model was conducted. Once they become matched, the unknown parameters of k_{rn}, k_{rw}, and S_s were determined. To examine their uncertainties, a sensitivity analysis of the parameters k_{rn} and k_{rw} towards the differential pressure was undertaken. Pressure gradient is insensitive when the parameter k_{rw} was above 0.5 at all values of the parameter k_{rn}. On the other hand, at all values of the parameter k_{rw}, pressure gradient is insensitive at the parameter k_{rn} above 0.1. This means the parameter k_{rn} is more sensitive than k_{rw}.

Figure 9 presents the CO_2-water relative permeability of the Ainoura specimens. As expected, the relative permeability of water decreased while that of CO_2 increased. Overall, CO_2 relative permeability at irreducible water saturation was observed to be lower than what we expected as it was about 15% of the water relative permeability at conditions of 100% water saturations. This indicated a lower displacement efficiency of the saturated water by the injected CO_2 in Ainoura Sandstones. The result may be attributed to heterogeneous bi-modal pore distribution of Ainoura Sandstones. Similarly, Bennion and Bachu (2005) observed that the pore size distribution of reservoir rocks critically affects CO_2-water relative permeabilities. In this kind of pore system, the CO_2-water displacement results in channel flow, yielding a non-uniform CO_2 flow in the system. All these imply that CO_2 flows preferentially in the smaller pores of the bi-modal pore system. Another factor that might be contributing to low relative permeability of CO_2 is the capillary pressure effect. By having a large fraction of micropores (more than 50%), the Ainoura specimens yielded relatively high capillary pressure. Therefore, its irreducible water saturation was high at about 45%. Capillary pressure acts as a barrier for CO_2 flow when very low injection rates applied.

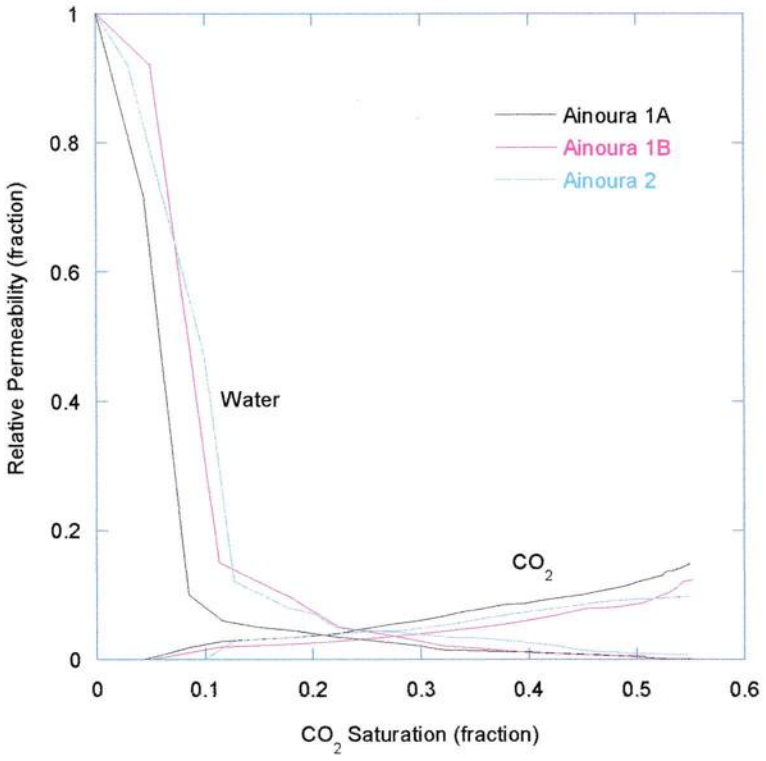

FIG. 9. End-point relative permeabilitiy of Ainoura sandstones versus CO_2 saturation.

Specific storage versus saturations

Figure 10 presents the change of specific storage of the Ainoura specimens with increasing CO_2 saturation. It was observed that the injection of CO_2 increased the specific storage of the specimen. Such a transient increase of specific storage beyond certain saturation was found at the same period of the significant increase of volumetric strain of the specimen. This suggested that the change of specific storage beyond certain CO_2 saturation is more pronounced as a mechanical response rather than just a hydraulic process. The specific storage increased by about 0.0004, 0.0003, and 0.0005 1/Pa for Ainoura 1A, 1B and 2, respectively.

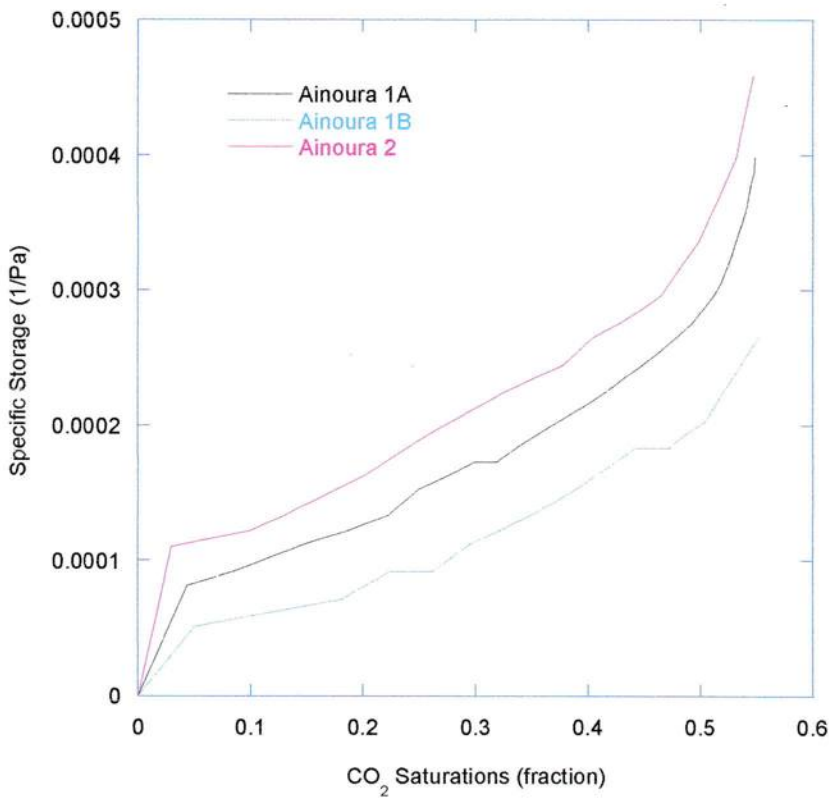

FIG. 10. Specific storage versus CO_2 saturation in Ainoura sandstone.

The validity of the specific storage obtained from the numerical analysis was also examined. The accuracy of specific storage of rock specimen is much affected by the storage capacity of the pump system. Tokunaga and Kameya (2003) introduced a dimensionless parameter, δ', described as the ratio of the pump's storage capacity to the specimen's specific storage:

$$\delta' = \frac{\delta}{L} = \frac{C_e}{S_s AL} \tag{7}$$

They suggested that the parameter Ss would have sufficient accuracy if the ratio, δ', is less than 0.3. In the numerical analysis, the ratio of the obtained Ss to the measured Ce was found to be between 0.00078 and 0.0187 (Figure 11). This clearly shows the ratios are below the ambient ratio of 0.3. However, the ambient ratio to examine accuracy of specific storage may be insufficient to implement in a transient flow from CO2-water drainage displacement system in reservoir condition. Further sensitivity analysis and poro-elasticity measurement to examine the accuracy of specific storage will be a subject of future investigation. Nonetheless, as preliminary validation to the numerical analysis, the use of ambient ratio of Tokunaga and Kameya (2003) was found acceptable.

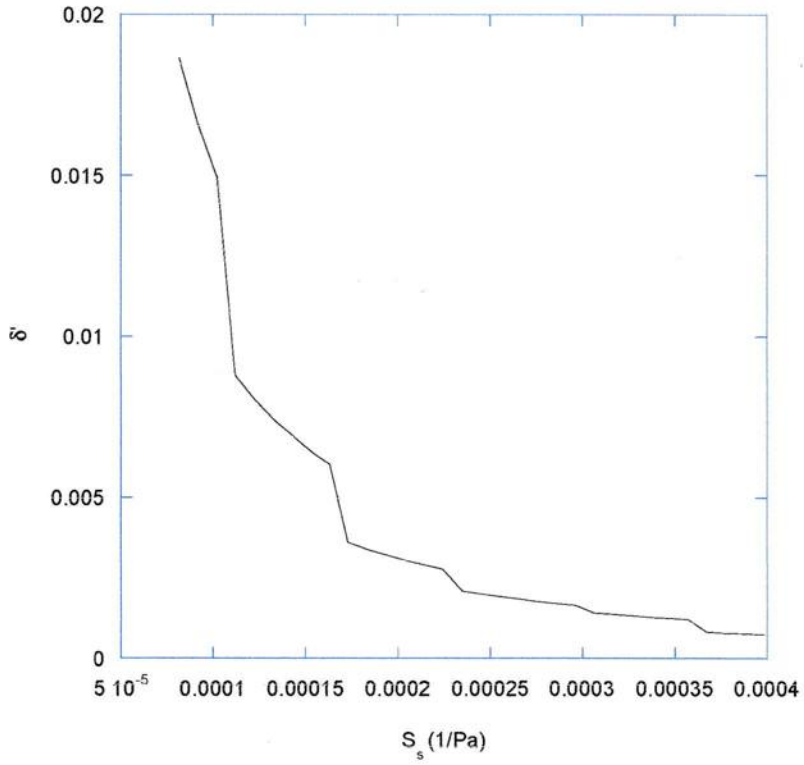

FIG. 11. Ratio of pump storage capacity to the Ainoura sandstone's storage capacity.

Change of Bulk Compressibility of Ainoura Sandstones during CO_2 injection

Since the Ainoura sandstone specimen is a porous body subjected to internal pore pressure and external confining pressure, its bulk compressibility of the specimen can be determined based on matrix compressibility and the increased pore compressibility during the injection of CO_2 injection. The matrix compressibility (C_m) of the specimens is about 2.54×10-5/MPa for typical sandstone (Zimmerman, 1991). Figure 12 presents the transient increase of bulk compressibility occurs at the beginning of

CO_2 injection. This corresponded to the transition from the displaced incompressible water flow to the displacing compressible CO2, in the specimen pores. After this period, overall, bulk compressibility of the specimen decreased with increasing pore pressure. Above a certain pressure, the bulk compressibility reached a plateau that is independent of the pore pressure. Figure 12 also shows the tested Ainoura 2 has larger bulk compressibility than the tested Ainoura 1. This is due to higher fraction of macropores in the Ainoura 2 resulted in more flow of CO_2, leading to higher pore pressure generated.

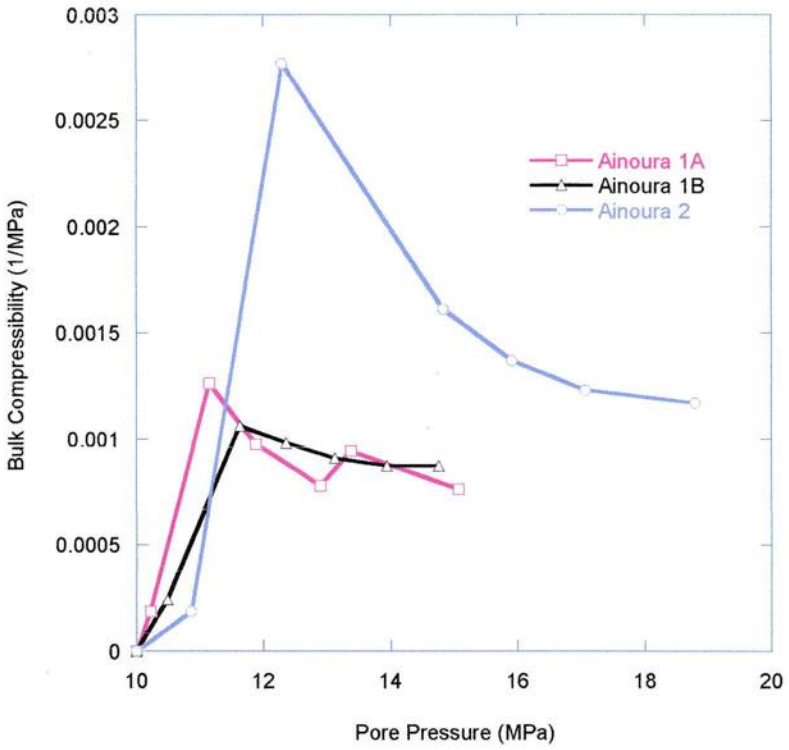

FIG. 12. Bulk compressibility changes as CO_2 injected into the rock specimens.

Effect of Pressure Margin on Volumetric Strain

The injection of CO_2 into the rock specimen increased its pore pressure and volumetric strain. As the experiments were constantly set at 20 MPa confining pressure, only the pore pressure increased from the 10 MPa initial pressure. If the pressure margin is defined as the gap pressure of the pore pressure to the confining pressure, the pressure margin decreased during the injection. The pressure margin was analysed in this study since it is a considerable parameter that might cause hydraulic fracturing. The initiation of hydraulic fracturing will occur when the pore pressure equals the confining pressure (Jaeger et al., 2007).

Figure 13 illustrates the relationship between the pressure margin and the volumetric strains measured during the experiments. As seen, the pressure margin increased as the volumetric strain increased. Beyond a certain pressure margin, the volumetric strains increased significantly. The transient increase of volumetric strain occurs at the transition of the incompressible water flow to the compressible CO_2 flow in the specimen pores, as observed in the second phase of the experiment. After that, the CO_2 did breakthrough the specimen, generating a higher increase of the volumetric strain. Given the trend of curves in Figure 13, the flow of CO_2 would generate a significant increase in volumetric strain when the pressure margins are above -9 MPa and -8 MPa for the Ainoura 2 and 1 samples, respectively. This means that the increased volumetric strain of the higher porosity specimen would occur slower than that of the lower porosity specimen. However, in the case of the magnitude of the strains generated, the specimen with higher porosity yielded a larger volumetric strain compared to a lower porosity sample. As a result, the generated pore pressure in the higher porosity specimen took a shorter time to reach the confining pressure level. The results suggested the benefit of lower porosity Ainoura sandstones in which they would have a higher specific storage for CO_2 but would generate lower deformation. It is noted that the lower deformation observed was induced by the injection at the very low flow rate applied in the experimental test. The very low flow rate was selected to mimic laminar flow in deep underground.

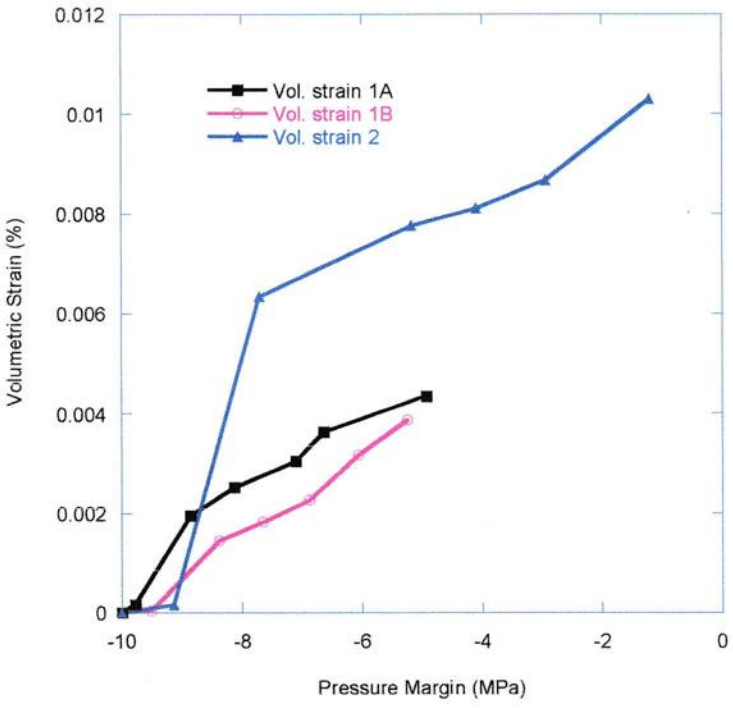

FIG. 13. Pressure margin of pore pressure to confining pressure versus volumetric of the specimens.

CONCLUSIONS

This paper presented experimental and numerical analysis to measure permeability and specific storage of sedimentary rock under the injection of CO2 in supercritical phase. Conclusions from this study are as follows:

- Ainoura sandstone has lower CO_2-water displacement efficiency indicated by low CO_2 relative permeability (only 15% of the relative permeability of water at 100% water saturation).
- The average capacity of Ainoura sandstones for storing supercritical CO_2 is estimated to be 3.74×10^{-4} 1/Pa within the experimental conditions applied.
- Ainoura sandstone appears to be effective in retaining the flow of supercritical CO_2 as it takes considerably long time to migrate through the sandstone.
- The injection of CO2 into the Ainoura sandstones has resulted in the increase of volumetric strains of the sandstones. Given by the direction of strains, the sandstones appear to be expanded during the injection;
- The expansion of the Ainoura sandstones is due to the decrease of effective pressure as the pore pressure induced by the injection increases and the confining pressure is set to be constant. The expansion initiates when the pressure margin between the pore pressure and the confining pressure is -9 MPa and -8 MPa for the Ainoura 1 and 2, respectively;

REFERENCES

Bennion, D.B., Bachu, S. (2005). The Impact of Interfacial Tension and Pore Size Distribution/Capillary Pressure Character on CO2 Relative Permeability at Reservoir Conditions in CO2-Brine Systems, SPE/DOE Symposium on Improved Oil Recovery, 22-26 April 2006, Tulsa, Oklahoma, USA SPE 99325.

Brace, W.F., Walsh, J.B., and Frangos, W.T. (1968). Permeability of granite under high pressure. Journal of Geophysical Research, 73(6), 2225-2236.

Carslaw, H. S., Jaeger, J.C.(1959). Conduction of Heat in Solids, Oxford University Press, London, P. 510.

Esaki, T., Zhang, M., Takeshita, A., and Mitani, Y.: Rigorous theoretical analysis of flow pump permeability test, Geotechnical Testing Journal 19, 241-246.

Jaeger, J.C., Cook, N.G.W., Zimmerman, R.W., (2007). Fundamentals of Rock Mechanics, Blackwell Publishing. Victoria Australia.

Morin, R.H., and Olsen, H.W. (1987). Theoretical analysis of the transient response from a constant flow rate hydraulic conductivity test, Water Resources Research 23, 1461-1470.

Müller, N.(2011). Supercritical CO2-brine relative permeability experiments in reservoir rocks—literature review and recommendations, Transport in Porous Media 87(2), 367 – 383.

Nakanishi, S., Mizuno, Y., Okumura, T., Miida, H., Shidahara, T., Hiramatsu, S. (2009). Methodology of CO2 aquifer storage capacity assessment in Japan and overview of the project, Energy Procedia, 1(1), Greenhouse Gas Control Technologies 9, Proceedings of the 9th International Conference on Greenhouse Gas Control Technologies (GHGT-9), 16-20 November 2008, Washington DC, USA, pp. 2639-2646.

Ogawa, T., Nakanishi, S., Shidahara, T., Okumura, T., Hayashi, E. (2011). Saline-aquifer CO2 sequestration in Japan-methodology of storage capacity assessment, International Journal of Greenhouse Gas Control 5(2) 318-326.

Olsen, H.W., Nichols, R.W., and Rice, T.L. (1985). Low-gradient permeability measurement in a Tri-axial system, Geotechnique 35, 145-157.

Perrin, J.-C., Benson, S.M. (2010). An experimental study on the influence of sub-core scale heterogeneities on CO2 distribution in reservoir rocks, Transport in Porous Media, Springer Netherlands, 93 – 109.

Perrin, J.-C., Krause, M., Kuo, C.-W., Miljkovic, L., Charoba, E., Benson, S.M. (2009). Core-scale experimental study of relative permeability properties of CO2 and brine in reservoir rocks, Energy Procedia 1(1), , Greenhouse Gas Control Technologies 9, Proceedings of the 9th International Conference on Greenhouse Gas Control Technologies (GHGT-9), Washington DC, USA, February 2009, pp. 3515-3522.

Shi, J.-Q,Xue,Z.,and Durucan, S. (2009). History matching of CO2 core flooding CT scan saturation profiles with porosity dependent capillary pressure, Energy Procedia, Volume 1, Issue 1, Greenhouse Gas Control Technologies 9, Proceedings of the 9th International Conference on Greenhouse Gas Control Technologies (GHGT-9), 16-20 November 2008, Washington DC, USA, pp. 3205-3211.

Song, I., Elphick, S.C., Main, I.G., Ngwenya, B.T., Odling, N.W., and Smyth, N.F. (2004). One-dimensional fluid diffusion induced by constant-rate flow injection: Theoretical analysis and application to the determination of fluid permeability and specific storage of a cored rock sample, J. Geophysical Resources 109, 1-9.

Takahashi, T., Ohsumi, T., Nakayama, K., Koide, K., Miida, H. (2009). Estimation of CO2 Aquifer Storage Potential in Japan, Energy Procedia, Volume 1, Issue 1, Greenhouse Gas Control Technologies 9, Proceedings of the 9th International Conference on Greenhouse Gas Control Technologies (GHGT-9), 16-20 November 2008, Washington DC, USA, pp. 2631-2638.

Tokunaga, T., Kameya, H. (2003). Determination of specific storage of a porous material from flow pump experiments: theoretical analysis and experimental evaluation, International Journal of Rock Mechanics and Mining Sciences 40(5), 739-745.

Van Genuchten, M. Th. (1980). A closed-form equation for predicting the hydraulic conductivity of unsaturated soils, Soil Science American Journal 44, 892.

Zhang, M., Takahashi, M., Morin, R.H., and Esaki, T. (2008). Evaluation and application of the transient-pulse technique for determining the hydraulic properties of low-permeability rocks—Part 2: experimental application. Geotech Test J 23, 91–99.

Zimmerman, R.W., (1991). Compressibility of sandstones. Developments in Petroleum Science, Vol. 29. Elsevier, New York.